Scientific Research Publishing

Journal of Materials Science and Chemical Engineering, 2024, 12, 1-19
https://www.scirp.org/journal/msce
ISSN Online: 2327-6053
ISSN Print: 2327-6045

TiO_2-PES Fibrous Composite Material for Ammonia Removal Using UV-A Photocatalyst

Anh Phuong Le Thi[1], Masaru Ohshiro[2], Takaomi Kobayashi[1*]

[1]Department of Science and Technology Innovation, Nagaoka University of Technology, Nagaoka, Japan
[2]Kasai Corporation, Niigata, Japan
Email: *takaomi@vos.nagaokaut.ac.jp

How to cite this paper: Thi, A.P.L., Ohshiro, M. and Kobayashi, T. (2024) TiO_2-PES Fibrous Composite Material for Ammonia Removal Using UV-A Photocatalyst. *Journal of Materials Science and Chemical Engineering*, **12**, 1-19.
https://doi.org/10.4236/msce.2024.121001

Received: December 2, 2023
Accepted: January 12, 2024
Published: January 15, 2024

Abstract

This study focused on the development and characterization of TiO_2-PES composite fibers with varying TiO_2 loading amounts using a phase inversion process. The resulting composite fibers exhibited a sponge-like structure with embedded TiO_2 nanoparticles within a polymer matrix. Their photocatalytic performance for ammonia removal from aqueous solutions under UV-A light exposure was thoroughly investigated. The findings revealed that PeTi8 composite fibers displayed superior adsorption capacity compared to other samples. Moreover, the study explored the impact of pH, light intensity, and catalyst dosage on the photocatalytic degradation of ammonia. Adsorption equilibrium isotherms closely followed the Langmuir model, with the results indicating a correlation between q_m values of 2.49 mg/g and the porous structure of the adsorbents. The research underscored the efficacy of TiO_2 composite fibers in the photocatalytic removal of aqueous NH_4^+ under UV-A light. Notably, increasing the distance between the photocatalyst and the light source resulted in de-creased hydroxyl radical concentration, influencing photocatalytic efficiency. These findings contribute to our understanding of TiO_2 composite fibers as promising photocatalysts for ammonia removal in water treatment applications.

Keywords

Ammonia Removal, Photocatalyst, TiO_2-PES Composite Fiber, Fibrous Material

1. Introduction

Ammonium-nitrogen (NH_4-N) serves as a nitrogen source conducive to plant growth, and it constitutes an integral component of fertilizers, which invariably

contain nitrogen in the form of either ammonia or its NH_4-N derived compounds. Numerous origins contribute to NH_4-N pollution, with municipal sewage serving as one notable source [1], industrial wastewater [2], landfill leachate [3] and agriculture discharges as well as agricultural residues [4]. The excessive release of NH_4-N into the environment via aquatic drainage gives rise to discernible repercussions on both aquatic ecosystems and human health. Elevated NH_4-N concentrations in water foster the proliferation of photosynthetic microorganisms, thus precipitating eutrophication, a phenomenon with potentially severe consequences. This process can engender a reduction in dissolved oxygen levels as a result of NH_4-N oxidation in water, thereby diminishing water quality and leading to the development of discolored and malodorous water bodies. These deleterious conditions can ultimately lead to mortality among aquatic flora and fauna. Moreover, the depletion or contamination of water resources due to pollution may exert adverse effects on economic growth and employment opportunities. Consequently, the imperative need for wastewater treatment and reuse has emerged as one of the most critical global water resource concerns.

To address this concern, extensive research endeavors have been undertaken to explore various ammonia removal techniques, encompassing biological processes [5], stripping [6], chemical precipitation [7], as well as the utilization of diverse separation materials such as ion exchange [5], adsorbents [8] [9], and membranes [10]. Each of these methods possesses its inherent advantages and disadvantages. For instance, biological processes necessitate substantial water volumes and stringent requirements pertaining to pH, carbon content, and dissolved oxygen conditions. Air stripping processes exhibit high efficacy in removing NH_4-N from wastewater; however, they may lead to the release of gaseous ammonia into the environment, potentially causing secondary pollution concerns [11]. The chemical precipitation method for NH_4-N removal has demonstrated an impressive capacity to achieve removal efficiencies exceeding 92% within a brief reaction timeframe. Furthermore, the by-products generated through this process hold potential utility as fertilizers. However, it is essential to note that this method entails substantial operational expenses and demands a considerable quantity of sediment agents. [12]. In contrast, absorbents and membrane-based approaches impose significant energy consumption [13] [14]. When juxtaposed with the aforementioned methodologies, photocatalysis emerges as a highly promising pollution control technology, characterized by its environmentally friendly attributes and remarkable efficacy in NH_4-N removal [15] [16] [17]. The pioneering utilization of TiO_2 photocatalysis for NH_4-N oxidation dates back to 1979, and since then, it has garnered substantial attention [17]-[22]. Furthermore, TiO_2 has consistently been employed as a photocatalyst for redox reactions and has been extensively documented in scientific literature [23] [24] [25] [26]. However, it is imperative to acknowledge that the use of TiO_2 particles as photocatalysts, particularly in slurry systems, poses challenges concerning the recovery of TiO_2 particles from the treated water medium [27]. The uncollected slurry can introduce environmental contamination concerns, which

necessitate resolution. Additionally, investigations into the toxicological aspects of TiO_2 have revealed its potential harm to both plants and animals [28]. Elevated concentrations of this material in surface water bodies could pose a substantial threat to aquatic ecosystems and environmental health.

The choice of an ideal substrate for immobilizing photocatalysts is paramount, as it must provide stable anchoring to prevent catalyst leaching and exhibit selective affinity for the targeted contaminants. Various materials have been explored as supports for photocatalysts, including glass, silica, ceramics, polymers [29] [30], activated carbon, alumina, zeolite, natural fiber composite [31], and stainless steel [32]. Notably, polymers such as Polyether Sulfone (PES) hold promise as substrates due to their high chemical and mechanical stability [33]. Furthermore, the hydrophobic nature of PES facilitates the concentration of inorganic contaminants on its surface, where photocatalysts are anchored. The substrate's architecture is critical in providing a high surface area. Wet spinning, as a method, is particularly appealing for the fabrication of micrometer (μm)-sized fibers with relatively substantial surface areas, thereby enabling the anchoring of a significant quantity of photocatalysts with minimal disruption to the fabrication process.

Building upon prior research findings, this study seeks to address the limitations associated with ammonia removal by investigating the use of fibrous TiO_2 composite materials. Recognizing the inherent drawbacks of TiO_2 powder, the objective is to harness the advantages of composite materials incorporating polymers. Prior research has demonstrated the efficacy of incorporating zeolites into polymer matrices for various applications, including heavy metal removal [34]. Our earlier investigations have revealed that polymer composites containing zeolites exhibit superior performance in heavy metal removal and decontamination efforts when compared to powdered zeolite. In these investigations, a specific polymeric material, polyether-sulfone (PES), was employed due to its exceptional mechanical properties, chemical stability, high heat resistance, and ease of processing. This article is primarily focused on the fabrication of TiO_2-PES composite fibers and their application in the photooxidation of ammonia for decontamination under light exposure. The investigation entails varying the loading amounts of TiO_2 embedded within the fibrous PES scaffold, with the aim of characterizing their suitability as materials for ammonia removal.

2. Material and Methods

2.1. Materials

TiO_2 nano powder was procured from Fujifilm Wako Pure Chemical Co., Ltd., with the X-ray Fluorescence (XRF) analysis revealing the following chemical composition in percentage values: CO_2: 14.6%, TiO_2: 85.0%, Na_2O: 0.284%, and Fe_2O_3: 0.024%. Prior to its incorporation with PES, the TiO_2 powder underwent a crushing process and was subsequently sieved through a No. 230 sieve. N-Methyl-2-pyrrolidone (NMP) and various other chemicals were acquired

from Nacalai Tesque Inc. (Japan) and utilized in their as-received state without additional purification. The polyethersulfone (PES) employed, specifically Ultrason E2010, was sourced from BASF Co. Ltd. (Germany). To prepare the Ammonium-Nitrogen solutions, ammonium bicarbonate (NH_4HCO_3) obtained from Nacalai Tesque Inc., Japan, was dissolved in distilled water, resulting in a working solution with a concentration of 1000 mg/L. Before conducting the adsorption experiments, the ammonium solution was diluted accordingly. In cases where 0.1 M HCl and 0.1 M NaOH solutions were employed, the pH values of the solutions were adjusted as necessary.

2.2. Fabricating TiO_2-PES Composite Fibers with Wet Spinning Process

In accordance with our previously established procedures [35] the wet-spinning process was employed to fabricate TiO_2-PES composite fibers by utilizing the phase inversion of a PES solution into solid PES [36]. Here, PES was dissolved in NMP at a concentration of 30 wt%. Subsequently, varying amounts of TiO_2 powder (2, 5, 8, and 10 wt%) relative to the weight of PES were introduced. The resultant mixture was extruded through a cylindrical needle with a 0.6 cm-diameter, and an applied pressure of 0.42 MPa was utilized to extrude it into a water coagulation bath maintained at 25˚C. Within this coagulation bath, the composite fibers took form and were subsequently rinsed in excess water at 60˚C to eliminate any residual NMP. Finally, the composite fibers were subjected to drying under vacuum conditions at 60˚C. The fibers produced at 30 wt% PES, with varying TiO_2 content of 0, 2, 5, 8, and 10 wt%, were denoted as PeTi0, PeTi2, PeTi5, PeTi8, and PeTi10, respectively.

2.3. Characterization of the Composite Fibers

To explore the alterations in fiber morphology, scanning electron microscopy (SEM) was conducted using a TM3030Plus HHTC instrument from Japan. The samples were sputter-coated with gold before examination, and imaging was carried out at an accelerating voltage of 15 kV. The surface area of both the TiO_2 and composite fibers was determined using the Brunauer-Emmer-Teller (BET) method, and the measurements were performed with a Tristar II 3020 apparatus (Micromeritics Inc., Tristar II, Shimizu, Japan). Prior to analysis, the samples were subjected to degassing under vacuum conditions overnight at 70˚C. X-ray diffraction (XRD) spectra of limonite and the composite fibers were acquired using a SmartLab X-ray diffractometer (Rigaku Corporation) equipped with Cu Kα radiation (λ = 1.5406 Å). The XRD patterns were recorded over a 2θ range spanning from 10˚ to 70˚, employing parameters of 40 kV and 30 mÅ. For component analysis of TiO_2 and composite fibers, an X-ray fluorescence analyzer (ZSX Primus II, Rigaku Corporation, Japan) was utilized. Pellets with a 10 mm diameter were fabricated from TiO_2, composite fibers, and an aluminum ring using a hydraulic press, applying a pressure of 450 kgf/cm^{-2} for the mea-

surements. The tensile strength of the TiO_2 composite fibers was determined with a load measurement device (LTTU500N, Minebea Co. Ltd., Japan) operating at 500 N and 23˚C with a relative humidity of 50%. The gauge length was set at 30 mm, and the crosshead speed was maintained at 2 mm/min. Five specimens were subjected to testing for each sample, and each specimen had a length of 50 mm. Initially, the diameter of each piece was measured using a micrometer (Mitutoyo 103 - 177, Japan) to calculate the cross-sectional surface area. The tensile strength and elongation were subsequently computed using the following equations: tensile strength (MPa) = maximum load/cross sectional area and elongation (%) = 100 × (elongation at rupture/initial gauge length). The density of the composite fibers was determined through the Archimedes method. A dry specimen with a known weight was immersed in excess water until equilibrium was reached with the specimen in the water. The density of the prepared specimens (ρ) was calculated using the formular:

$$\rho = \frac{W_s}{W_s - W_w} \times (\rho_0 - d) \tag{1}$$

where ρ is the density (g/cm^3), W_s denotes the specimen weight in air (g), W_w represents the specimen mass in ethanol (g), ρ_0 is the density of ethanol (g/cm^3), and d is the density of air (g/cm^3).

Zeta potential measurements were conducted on both the TiO_2 powder and the composite fibers (after they were ground into powder form) within a pH range of 5 - 11. This analysis was carried out using a Zeta-potential analyzer (ELSE1NGK; Otsuka Electronics Co. Ltd., Japan), with distilled water employed as the dispersion medium. The medium's pH was adjusted through titration, utilizing 0.1 M HCl and 0.1 M NaOH solutions, to determine the zeta potential of the TiO_2 powder and the composite fibers.

2.4. Photocatalytic Adsorption Process of Ammonium Ion in the Batch Mode

The photocatalytic oxidation of ammonia in water, employing either TiO_2 composite fiber or TiO_2 powders, was carried out within a batch water medium. This reaction was conducted under exposure to light, specifically illuminated using a UV-A Hg lamp with a power rating of 25 W, positioned at a fixed distance of 10 cm above the central point of a pyrex glass reactor. The reactor possessed a 5 L capacity, and the average light intensity throughout the experiments approximated 300 μW/cm^2. To ensure the accuracy of the experiments, the entire system was shielded by an aluminum foil sheet, effectively preventing any interference from external light sources. For the purpose of maintaining well-mixed solutions during the experiments, circulating water was employed. Additionally, an air diffuser was installed at the base of the reactor tube as part of the experimental setup.

To conduct the ammonium adsorption experiments, either 10 g of TiO_2 composite fiber or 1 g of TiO_2 nano powder was individually introduced into a 1 L

solution containing $NH_4HCO_3^-$. Subsequently, the mixtures were exposed to UV-A lamp irradiation at an intensity of 300 μW/cm² for a duration of 12 hours at a temperature of 25˚C. The adsorption kinetics of NH_4^+ were examined using the chosen adsorbents, namely TiO_2, PeTi2, PeTi5, PeTi8, and PeTi10, across varying concentrations ranging from 0.27 to 2.7 mM (equivalent to 5 to 50 ppm). During the experiments, small sample solutions, each comprising less than 10 mL, were withdrawn and stored in opaque vials to minimize potential interference from indoor fluorescent lighting before subsequent analyses. The concentrations of NH_4^+, NO_2^-, were determined using a UV-visible spectrophotometer (Jasco V-750). Specifically, NO_3^- concentrations were ascertained using the NO_3^- 11S LAQUATwin Kit designed for nitrate measurements. The concentrations of NH_4^+, NO_2^-, and NO_3^- were calculated using five-point external standard calibration curves. Standard solutions were freshly prepared on a daily basis, and the analysis of standards was consistently repeated daily. The NH_4^+ ions in the samples were detected through a colorimetric method following the 4500-NH_3 F-Phenate method. The colored samples were assessed for absorbance at 640 nm. For the determination of NO_2^- content, a Griess assay was employed, utilizing N-(1-naphthyl)ethylenediamine (NED) as a coupling component in the reaction. The colored samples were analyzed for absorbance at 540 nm. The adsorption equilibrium isotherms were assessed using both the Langmuir and Freundlich models. In the Langmuir model, the equation took the form:

$$\frac{C_e}{q_e} = \frac{C_e}{q_m} + \frac{1}{q_m K_L} \quad (2),$$

q_e is equilibrium adsorption amount (mmol/g), q_m is maximum adsorption capacity (mmol/g), and K_L is Langmuir constant.

Conversely, for the Freundlich model, the equation adopted was:

$$\ln(q_e) = \ln(K_F) + \frac{1}{n}\ln(C_e) \quad (3),$$

K_F, and n are Freundlich constant.

It is well-established that the degradation rate is associated with the formation of hydroxyl radicals (OH•) on the catalyst surface. The quantity of hydroxyl radicals generated is contingent upon several factors, including the catalyst type, catalyst dosage, pH value, and light intensity. In this particular study, the impact of pH, catalyst dosage, and light intensity were also thoroughly investigated. In the context of photo exposure experiments, 10 g of the composite fibers were brought into contact with a 1 L aqueous ammonia solution containing 35 ppm concentration. Subsequently, the UV-A lamp was exposed to the solution for a duration of 96 hours.

3. Results and Discussion

3.1. TiO_2 Composite Fiber Characterization

Figure 1 provides an insight into the morphology of TiO_2-PES composite fibers

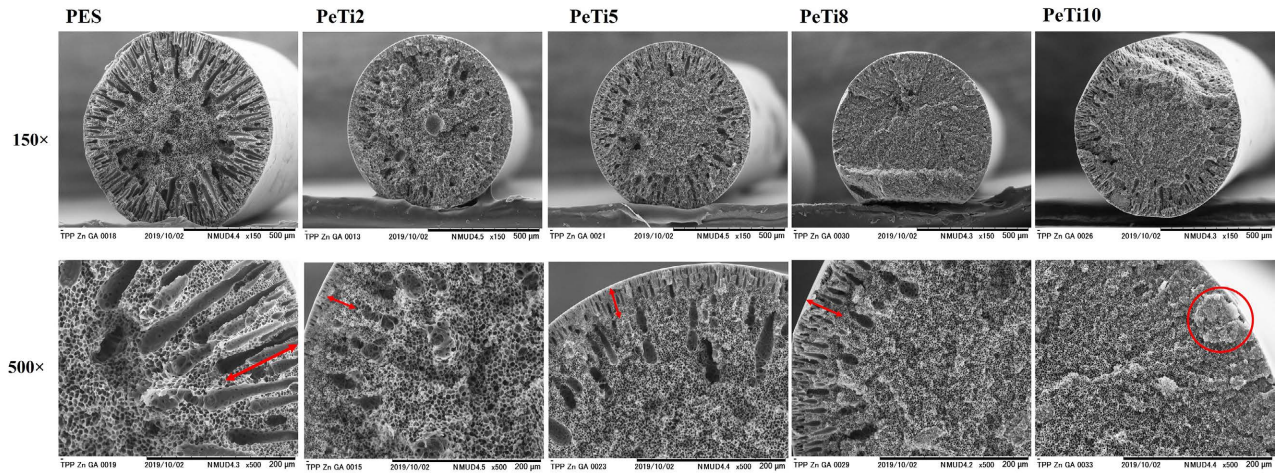

Figure 1. Cross-section of PES fiber and TiO_2 composite fibers at 150 and 500 magnifications.

loaded with varying amounts of TiO_2 within PES fibers. These resultant fibers exhibited an approximate diameter of 500 μm. Examination of their cross-section revealed a highly porous, sponge-like structure with pores smaller than 5 μm at the central region. This structure displayed a finger-like, elongated pore distribution extending from the fiber's core to its surface. However, it's noteworthy that the larger finger-like pores transitioned into much smaller structures when the TiO_2 content ranged from 2 to 8 wt%, and they were distributed at approximately 50 μm from the fiber surface. Remarkably, when the TiO_2 content reached 10 wt%, these larger pores nearly vanished, and the fiber cross-section exhibited a generally dense and spongy appearance. These observations suggest that, when the TiO_2 dispersion solution is added to the PES and coagulated in water, the coagulation rate slows down with increasing TiO_2 content, and the solvent exchange rate also becomes less rapid. Furthermore, the XRF elemental analysis presented in **Table 1** reveals that the TiO_2 content closely aligns with the quantity of added TiO_2. As the TiO_2 content in the composite fiber increases, the density values exhibit a trend of 0.81, 0.83, 0.87, and 1.07 for 2, 5, 8, and 10 wt% respectively. The BET surface area values, determined through nitrogen adsorption, demonstrate a pattern where the surface area increases for PeTi2, PeTi5, and PeTi8, and then decreases in PeTi10. These findings indicate that the incremental addition of TiO_2 in the composite influences the surface area of the resulting fibers, with the highest surface area noted at 8 wt%. At a TiO_2 content of 10 wt% in the composite fibers, the surface area exhibited a slight decrease, suggesting the initiation of an aggregation process of TiO_2 nano powder. These results are further corroborated by the SEM cross-section images shown in **Figure 1**.

In **Figure 2**, N_2 adsorption is presented at various relative pressures for each composite fiber. The results clearly indicate that the N_2 adsorption amount exhibited an increase in proportion to the TiO_2 loading. Notably, the composite fibers displayed a substantial increase in N_2 adsorption, particularly under a relative pressure of 0.1. To provide a quantitative perspective, the BET surface areas

of PES and the composite fibers, including PeTi2, PeTi5, PeTi8, and PeTi10, were measured and found to be 18.09, 25.93, 48.19, and 37.76 m^2/g, respectively. As shown in **Figure 3**, XRD patterns for both TiO_2 and the TiO_2 composite fibers are depicted. The main peaks, discerned at 25.3˚, 37.9˚, 48.3˚, 53.9˚, 54.9˚, 62.7˚, 68.84˚, 70.1˚, and 75.03˚, correspond to the facets (101), (004), (200), (105), (211), (204), (113), (220), and (215), respectively. These peak positions align with the characteristic pattern of tetragonal anatase TiO_2 [37]. Importantly, no other diffraction peaks were observed in the XRD pattern, signifying the absence of any chemical reactions between TiO_2 and the PES polymer during the synthesis process.

Table 1. Properties of composites fibers, PES fiber, and TiO_2.

Sample	TiO_2 content (%)	Density (g/cm^3)	BET surface area (m^2/g)	Pore size (nm)	Tensile strength (MPa)	Zeta potential at pH 9
PES	0	0.8	1.73	8.3	11.4	−6.7
PT2	2	0.81	18.1	7.9	10.1	−9.4
PT5	5	0.83	25.9	6.8	10.1	−8.6
PT8	8	0.87	48.2	6.5	9.7	−7.8
PT10	10	1.07	37.8	5.7	7.6	−10.4
TiO_2	100	-	204.9	7.4	-	−18.3

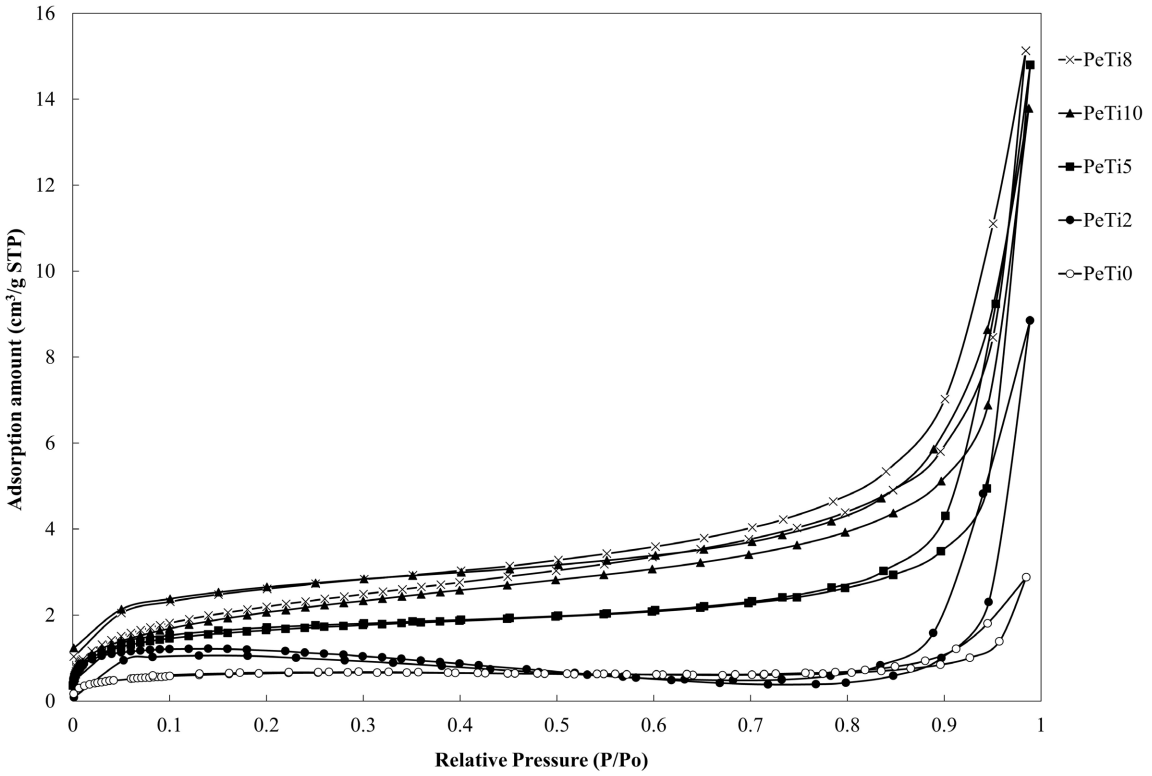

Figure 2. N_2 adsorption of PES and the TiO_2-PES composite fiber.

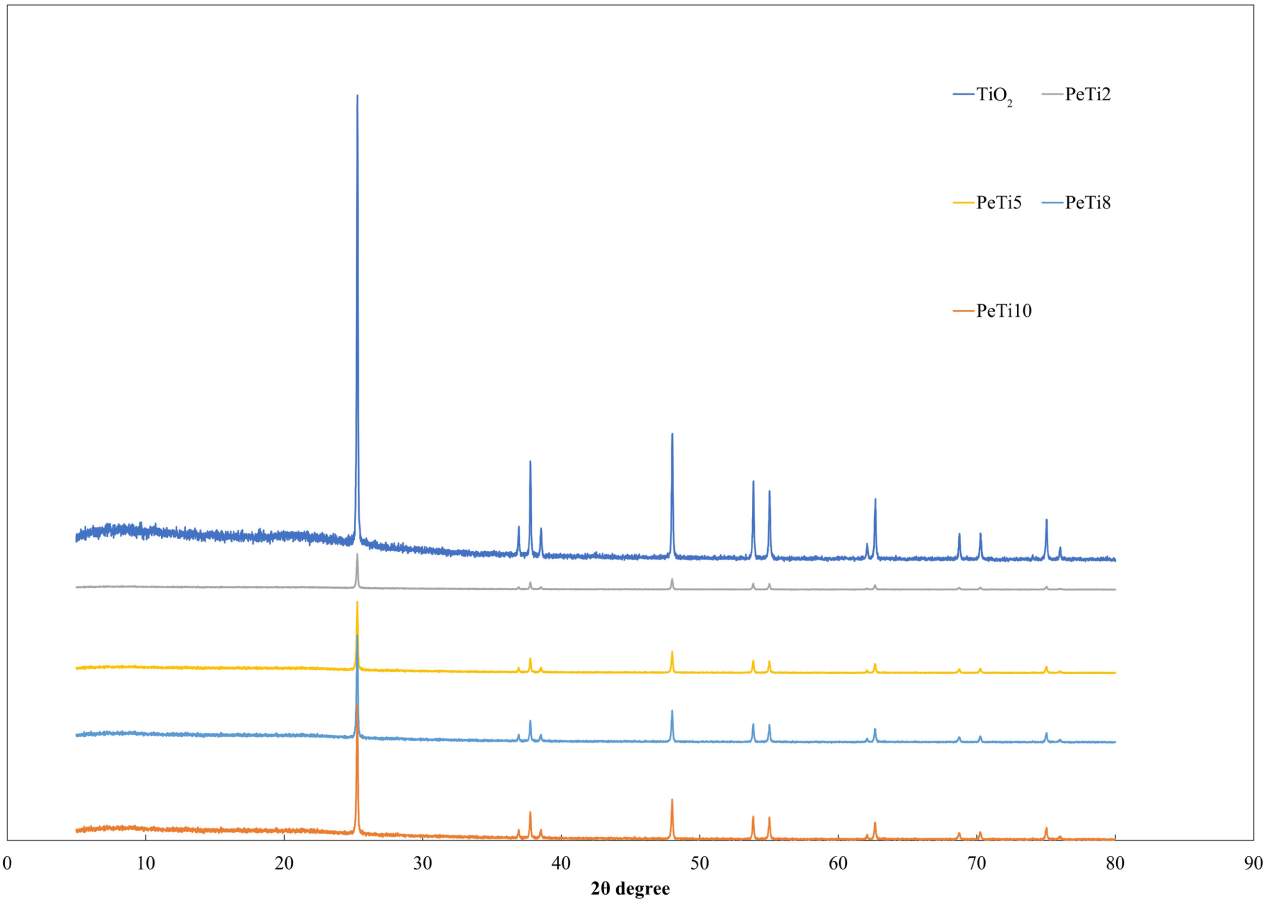

Figure 3. XRD spectra of the TiO_2-PES composite fiber.

3.2. Adsorbent Behavior of Composite Fiber to Ammonium under the UV-A Lamp Exposure

Figure 4. pH effect on the NH_4^+ removal by using photocatalyst method with TiO_2 composite fibers. The ammonia photo-oxidation process was conducted across a range of pH values, spanning from 5 to 11. This pH variation was achieved by the addition of either 0.1 N NaOH or 0.1 N HCl solutions, and the results are depicted in the accompanying **Figure 4**. pH is a crucial parameter in the photocatalytic oxidation of ammonium, as it plays a role in adjusting the surface charge of the photocatalyst. The results clearly illustrate that ammonia removal efficiency was notably lower in acidic pH conditions. This phenomenon can be attributed to the inhibition of hydroxide group production necessary for the formation of hydroxyl radicals under acidic conditions. Moreover, the adsorption of ammonia molecules onto the photocatalyst surface decreased due to the positively charged nature of the photocatalyst surface, leading to repulsive forces. Consequently, the degradation efficiency of ammonia diminishes under acidic pH. Conversely, the removal efficiency of ammonia exhibited a substantial increase, rising from 18.5% to 60%, as the pH was raised from 5 to 11 during a 12-hour period under UV irradiation. This increase can be attributed to the higher concentration of hydroxide ions generated under alkaline pH conditions.

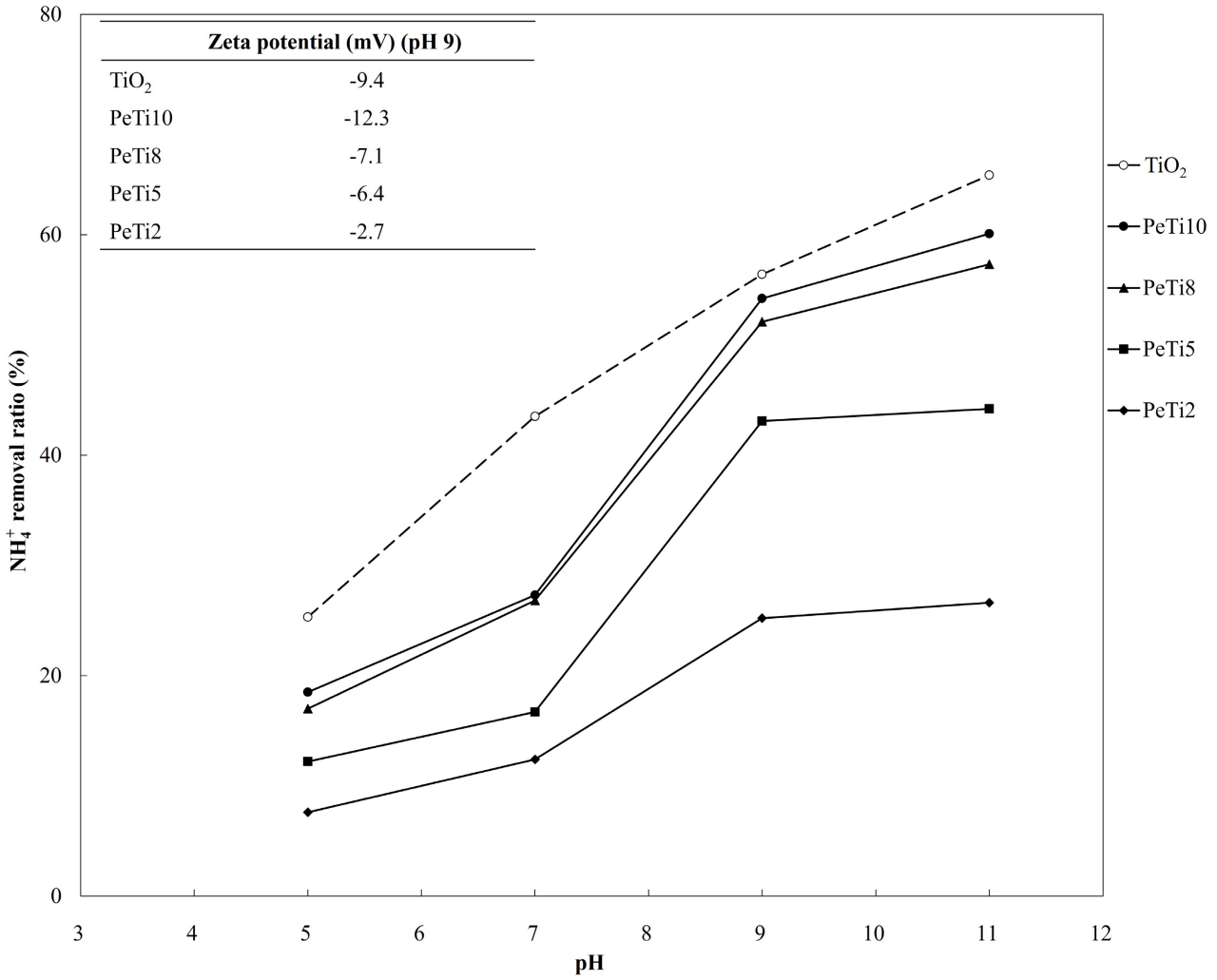

Figure 4. pH effect on the NH_4^+ removal by using photocatalyst method with TiO_2 composite fibers.

These hydroxide ions facilitate the reaction with the photo-generated holes, resulting in the formation of hydroxyl radicals. For practical and environmentally friendly considerations, this study chose to operate at pH 8, which demonstrated high removal efficiency, reaching approximately 50%.

Figure 5 illustrates the adsorption isotherms for ammonium on TiO_2 and the TiO_2 composite fibers. Equilibrium concentration data were analyzed using two isothermal models, Langmuir and Freundlich, and the results are presented in Table 2. In the adsorption isotherm, the data fit well to the Langmuir model, with correlation efficiency (R^2) values ranging from 0.9401 to 0.9936, while the Freundlich model yielded R^2 values in the range of 0.8345 to 0.9601. These results suggest that the saturation adsorption on TiO_2 sites within the fibers forms a monolayer. The maximum adsorption capacity (q_m) for ammonium ions on TiO_2 and composite fibers followed this order: PeTi10 > PeTi8 > PeTi5 > PeTi2. This indicates that q_m values are dependent on the porous structure of the adsorbents.

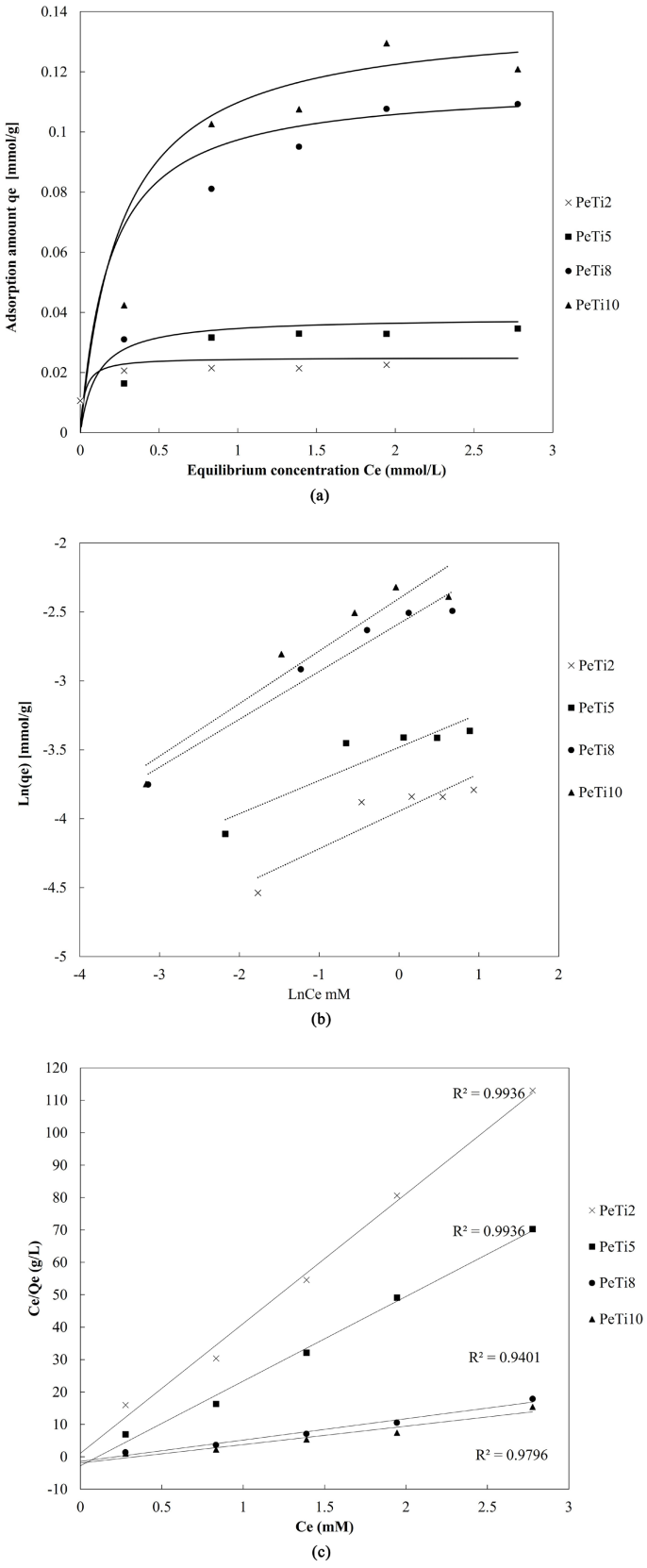

Figure 5. Adsorption isotherm of NH_4^+ by using the TiO_2 composite fibers (a), Freundlich adsorption plots (b), Langmuir adsorption isotherm plots (c).

Table 2. Parameters on Langmuir and Freundlich of ammonium adsorption by the composite fibers.

Isotherm models parameter			
PeTi2	Langmuir	q_m (mg/g)	0.43
		K_L (L/mmol)	37.54
		R^2	0.99
	Freundlich	K_F	66.2
		$1/n$	0.07
		R^2	0.83
PeTi5	Langmuir	q_m (mmol/g)	0.69
		K_L (L/mmol)	9.4
		R^2	0.99
	Freundlich	K_F	74.7
		$1/n$	0.07
		R^2	0.84
PeTi8	Langmuir	q_m (mmol/g)	2.09
		K_L (L/mmol)	5.3
		R^2	0.98
	Freundlich	K_F	50.1
		$1/n$	0.13
		R^2	0.92
PeTi10	Langmuir	q_m (mmol/g)	2.49
		K_L (L/mmol)	3.8
		R^2	0.94
	Freundlich	K_F	47.2
		$1/n$	0.16
		R^2	0.85

The photocatalytic performance of TiO_2 and the composite fibers was evaluated through the degradation of NH_4^+ in an aqueous solution.

In Figure 6, the adsorption of NH_4^+ on TiO_2 and PeTi8 was significantly enhanced compared to other samples, indicating that the PeTi8 sample possesses more active sites on its surface. To optimize reaction conditions, the effects of photocatalyst exposure time and illumination intensity on the photocatalytic removal of aqueous NH_4^+ by TiO_2 and TiO_2 composite fibers under a UV-A lamp were further investigated. Figure 6 demonstrates the decrease in aqueous NH_4^+ concentration when treated with TiO_2 and TiO_2 composite fibers, starting with an initial solution pH of 8 and a light intensity of 300 μW/cm^2, while the

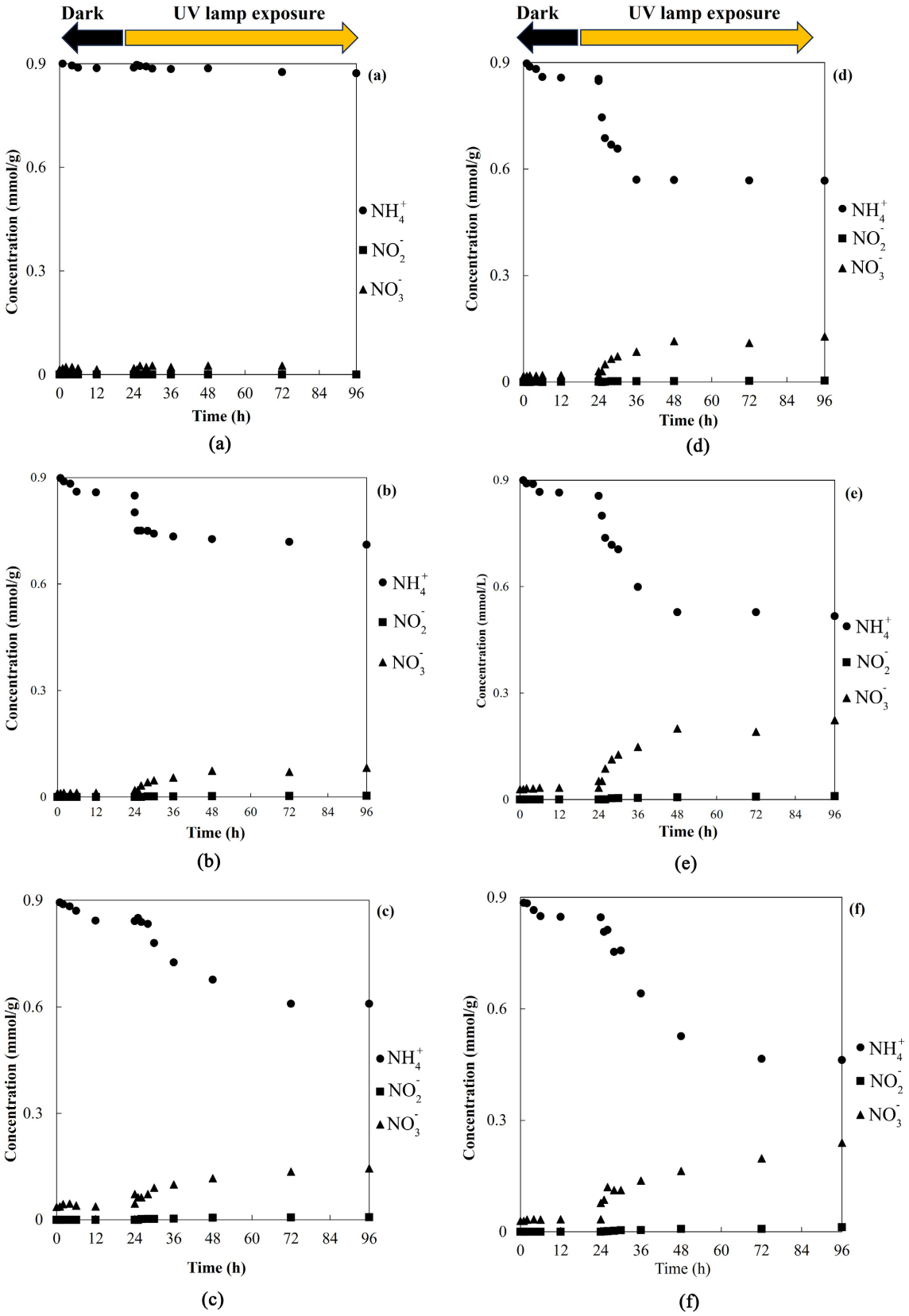

Figure 6. Conversion concentration between NH_4^+, NO_2^-, and NO_3^- when exposed to UV-A lamp for 96 hours. PeTi0 (a), PeTi2 (b), PeTi5 (c), PeTi7 (d), TiO_2 (f).

photocatalyst dosage was fixed at 10 g for TiO_2 composite fibers and 1 g of TiO_2 nano powder. As the TiO_2 content in the composite fibers changed, the removal of aqueous NH_4^+ initially decreased slowly in the absence of light. However, the removal dramatically decreased when the UV-A lamp was activated, observed between 25 to 36 hours. This phenomenon was consistent across all TiO_2 composite fibers. In cases of composite fibers with lower TiO_2 content, the production of reactive oxygen species was limited, affecting their photocatalytic performance. **Figure 6(b)** confirms this observation, as NH_4^+ concentration stabilized after 24 hours of exposure under the UV-A lamp, reaching 0.7 mmol/g. In the case of the highest TiO_2 content in the composite fiber, PeTi10, the NH_4^+ concentration was 0.5 mmol/g higher than the tank content of 10 g of PeTi8, which recorded 0.46 mmol/g, due to aggregation within the fiber structures. On the other hand, the results obtained from TiO_2 nano powder exhibited good adsorption ability in the first 6 hours when the UV-A lamp was turned on, but the removal ability gradually decreased and stabilized after 12 hours of exposure under irradiation. Compared to PeTi0, PES fiber showed no adsorption ability for NH_4^+. Additionally, **Figure 6** also presents the concentrations of photoconversion products, NO_2^- and NO_3^-, during the photocatalytic process. The high removal ratio of aqueous NH_4^+ and the presence of oxidation byproducts (NO_3^- and NO_2^-) could not be attributed to the weak volatilization of aqueous NH_4^+ under illumination. The results clearly demonstrate that TiO_2 composite fibers can effectively photo-catalytically remove aqueous NH_4^+ under the UV-A lamp. The higher NO_3^- yields in the tank content of 1 g of TiO_2 and 10 g of PeTi8 and PeTi10 compared to PeTi2 and PeTi5 are attributed to the appearance of TiO_2 in the photocatalyst process, as documented in previous research. These higher NO_3^- yields provide evidence that heterogeneous reactions dominate at higher TiO_2 concentrations.

Figure 7 depicts the variation in aqueous NH_4^+ concentration when treated with TiO_2 and TiO_2 composite fibers under a UV-A lamp with different tank volumes. Altering the tank volume affects the interaction distance between the light source and the pollutant, providing insights into the impact of light intensity at varying distances. With the same initial concentration of NH_4^+ in the aqueous solution and a consistent dosage of 10 g, the tank with a 0.25 L volume demonstrated effective NH_4^+ removal. Conversely, in the 2 L volume tank, the larger volume limited the utilization of photons in the solution, resulting in a less effective photocatalytic performance. The rate at which photocatalysis activates and forms electron-hole pairs in photochemical reactions is significantly influenced by the intensity of light. The efficiency of pollutant degradation depends on the distribution of light intensity within the reactor.

To explore the impact of light intensity on photocatalytic efficiency at different distances (2 cm, 5 cm, 10 cm, 15 cm, and 20 cm), all experiments were conducted under identical conditions, and the results are presented in **Figure 8**. Clearly, as the distance between the photocatalyst (PeTi8) and the light source

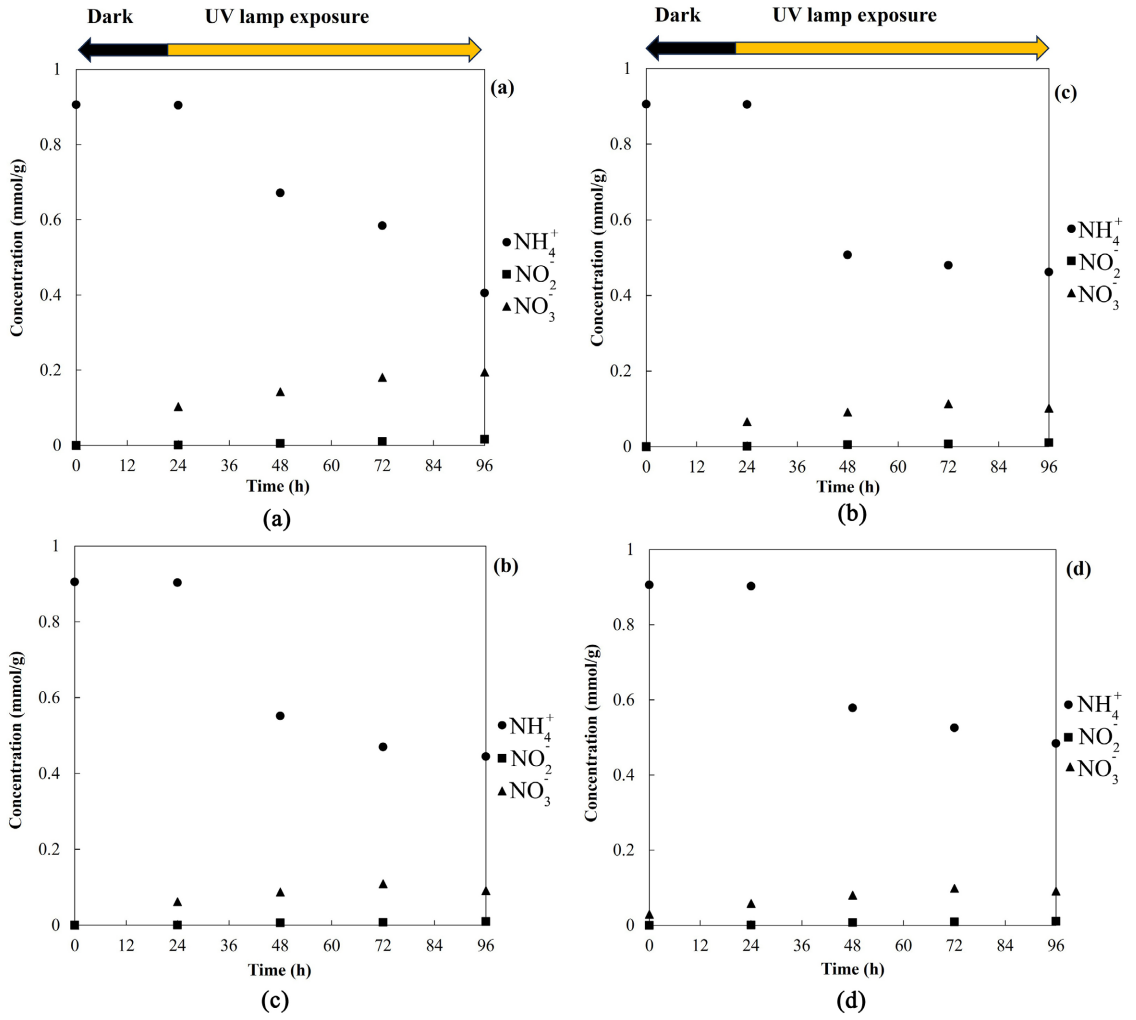

Figure 7. Conversion of concentration between NH_4^+, NO_2^-, and NO_3^- exposed to UV-A lamp with changing the tank volume. The PeTi8 composite were used, 0.5 L (a), 1 L (b), 1.5 L (c), 2 L (d).

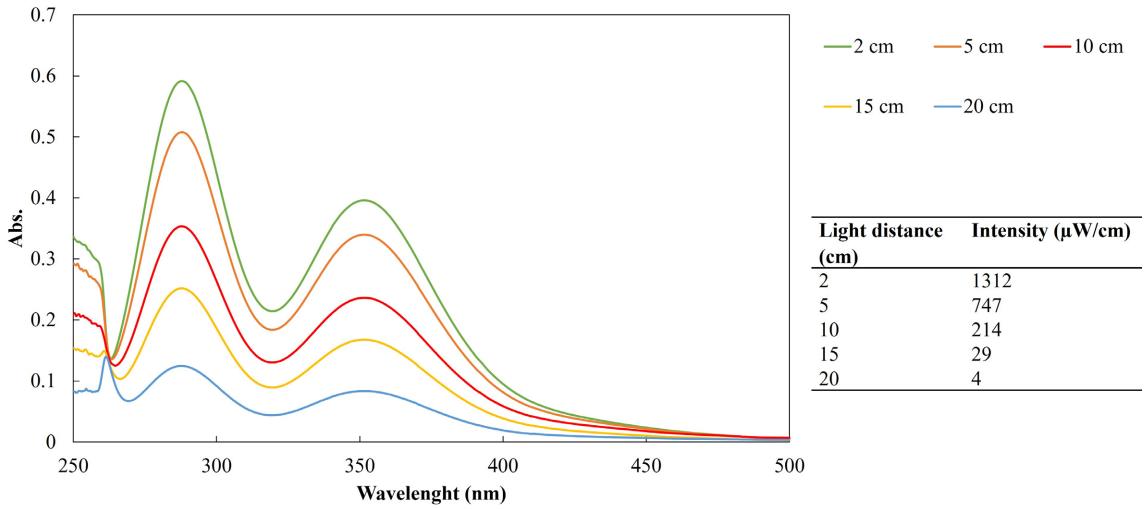

Light distance (cm)	Intensity (μW/cm)
2	1312
5	747
10	214
15	29
20	4

Figure 8. Distance dependent absorption spectra for the photocatalytic degradation of PeTi8 under UV-A light irradiation.

increases, the concentration of hydroxyl radicals (OH•) decreases. Generally, the distance between the light source and the photocatalyst has a significant effect on the reaction kinetics. It was observed that an increased distance led to a reduction in the rate constant, resulting in decreased catalyst activation and diminished photocatalytic degradation of ammonia. Figure 8 presents the OH• concentration at different distances and light intensities after 12 hours of initiating the reaction. Throughout the photocatalyst experiments, a certain quantity of hydroxyl radicals is produced. Changing the distance of the light source also impacts the ability to generate hydroxyl radicals in the aqueous environment. An experiment was conducted under the same conditions to assess the amount of hydroxyl radicals generated when altering the lamp distance from the catalyst. The results, as shown in Figure 8, indicate that as the distance of the lamp increases, the concentration of hydroxyl radicals decreases, with virtually no hydroxyl radicals being produced at a distance of 20 cm.

4. Conclusion

In conclusion, the TiO_2-PES composite fibers containing different loading amounts of TiO_2 were prepared using phase inversion. The properties of the composite fibers and adsorption behavior were investigated to characterize them on porous adsorbents. These composite fibers had sponge-like structures and embedded TiO_2 nanoparticles on a polymer matrix. The photocatalytic performance of the TiO_2 composite fibers and TiO_2 nanoparticles was evaluated. The removal of ammonia from aqueous solutions under UV-A light exposure demonstrated that PeTi8 composite fibers had higher adsorption capacity compared to other samples. The study also explored the effects of pH, light intensity, and catalyst dosage on the photocatalytic degradation of ammonia. The adsorption equilibrium isotherms for ammonium were well-fitted to the Langmuir model, and the results indicated that the qm values (maximum adsorption capacity) depended on the porous structure of the adsorbents. The research highlighted the ability of TiO_2 composite fibers to photocatalytically remove aqueous NH_4^+ under UV-A light. It was observed that increasing the distance between the photocatalyst and the light source led to a decrease in hydroxyl radical concentration, affecting the photocatalytic performance.

Acknowledgements

The authors express their sincere gratitude to the Kobayashi Laboratory and the Analysis Center at Nagaoka University of Technology for their indispensable aid in carrying out the XRD measurements and various experiments throughout the entire research endeavor. The invaluable support provided by the members has played a pivotal role in the successful culmination of this study.

Conflicts of Interest

The authors declare no conflicts of interest regarding the publication of this paper.

References

[1] Yang, Y., Zhang, S., Yang, A., Li, J., Zhang, L. and Peng, Y. (2020) Enhancing the Nitrogen Removal of Anammox by Treating Municipal Wastewater with Sludge Fermentation Products in a Continuous Flow Reactor. *Bioresource Technology*, **310**, Article ID: 123468. https://doi.org/10.1016/j.biortech.2020.123468

[2] Wu, H., Fan, J., Chen, W. and Yang, C. (2020) Dielectric Barrier Discharge-Coupled Fe-Based Zeolite to Remove Ammonia Nitrogen and Phenol Pollutants from Water. *Separation and Purification Technology*, **243**, Article ID: 116344. https://doi.org/10.1016/j.seppur.2019.116344

[3] Mojiri, A., Zhou, J.L., Ratnaweera, H., Ohashi, A., Ozaki, N., Kindaichi, T. and Asakura, H. (2020) Treatment of Landfill Leachate with Different Techniques: An Overview. *Water Reuse*, **11**, 66-96. https://doi.org/10.2166/wrd.2020.079

[4] Insausti, M., Timmis, R., Kinnersley, R. and Rufino, M.C. (2020) Advances in Sensing Ammonia from Agricultural Sources. *Science of the Total Environment*, **706**, Article ID: 135124. https://doi.org/10.1016/j.scitotenv.2019.135124

[5] Ricardo, A.R., Carvalho, G., Velizarov, S., Crespo, J.G. and Reis, M.A.M. (2012) Kinetics of Nitrate and Perchlorate Removal and Biofilm Stratification in an Ion Exchange Membrane Bioreactor. *Water Research*, **46**, 4556-4568. https://doi.org/10.1016/j.watres.2012.05.045

[6] Değermenci, N., Ata, O.N. and Yildız, E. (2012) Ammonia Removal by Air Stripping in a Semi-Batch Jet Loop Reactor. *Journal of Industrial and Engineering Chemistry*, **18**, 399-404. https://doi.org/10.1016/j.watres.2012.05.045

[7] Huang, H., Song, Q., Wang, W., Wu, S. and Dai, J. (2012) Treatment of Anaerobic Digester Effluents of Nylon Wastewater through Chemical Precipitation and a Sequencing Batch Reactor Process. *Journal of Environmental Management*, **101**, 68-74. https://doi.org/10.1016/j.jenvman.2011.12.035

[8] Sharifnia, S., Khadivi, M.A., Shojaeimehr, T. and Shavisi, Y. (2016) Characterization, Isotherm and Kinetic Studies for Ammonium Ion Adsorption by Light Expanded Clay Aggregate (LECA). *Journal of Saudi Chemical Society*, **20**, S342-S351. https://doi.org/10.1016/j.jscs.2012.12.003

[9] Huo, H., Lin, H., Dong, Y., Cheng, H., Wang, H. and Cao, L. 2012) Ammonia-Nitrogen and Phosphates Sorption from Simulated Reclaimed Waters by Modified Clinoptilolite. *Journal of Hazardous Materials*, **229-230**, 292-297. https://doi.org/10.1016/j.jhazmat.2012.06.001

[10] Stoquart, C., Servais, P., Bérubé, P.R. and Barbeau, B. (2012) Hybrid Membrane Processes Using Activated Carbon Treatment for Drinking Water: A Review. *Journal of Membrane Science*, **411-412**, 1-12. https://doi.org/10.1016/j.memsci.2012.04.012

[11] Zangeneh, A., Sabzalipour, S., Takdatsan, A., Yengejeh, R.J. and Khafaie, M.A. (2021) Ammonia Removal Form Municipal Wastewater by Air Stripping Process: An Experimental Study. *South African Journal of Chemical Engineering*, **36**, 134-141. https://doi.org/10.1016/j.sajce.2021.03.001

[12] Shu, N., Wang, X., Bi, Q., Zhao, T. and Han, Y. (2017) Disrupted Topologic Efficiency of White Matter Structural Connectome in Individuals with Subjective Cognitive Decline. *Radiology*, **286**, 229-238. https://doi.org/10.1148/radiol.2017162696

[13] Zhang, Y., Yin, S., Li, H., Liu, J., Li, S. and Zhang, L. (2022) Treatment of Ammonia-Nitrogen Wastewater by the Ultrasonic Strengthened Break Point Chlorination Method. *Journal of Water Process Engineering*, **45**, Article ID: 102501. https://doi.org/10.1016/j.jwpe.2021.102501

[14] Assawasaengrat, P. and Rueangdechawiwat, R. (2019) Adsorption of Ammonia Nitrogen in Aqueous Solution Using Zeolite A. *IOP Conference Series: Materials Science and Engineering*, **639**, Article ID: 012050. https://doi.org/10.1088/1757-899X/639/1/012050

[15] Saravanan, A., Kumar, P.S., Vo, D.V.N., Yaashikaa, P.R., Karishma, S., Jeevanantham, S., Gayathri, B. and Bharathi, V.D. (2021) Photocatalysis for Removal of Environmental Pollutants and Fuel Production: A Review. *Environmental Chemistry Letters*, **19**, 441-463. https://doi.org/10.1007/s10311-020-01077-8

[16] Parangi, T. and Mishra, M.K. (2019) Titania Nanoparticles as Modified Photocatalysts: A Review on Design and Development. *Comments on Inorganic Chemistry*, **39**, 90-126. https://doi.org/10.1080/02603594.2019.1592751

[17] Li, H., Cao, Y., Liu, P., Li, Y., Zhou, A., Ye, F., Xue, S. and Yue, X. (2022) Ammonia-Nitrogen Removal from Water with gC3N4-rGO-TiO_2 Z-Scheme System via Photocatalytic Nitrification-Denitrification Process. *Environmental Research*, **205**, Article ID: 112434. https://doi.org/10.1016/j.envres.2021.112434

[18] Mozzanega, H., Herrmann, J.M. and Pichat, P. (1979) Ammonia Oxidation over UV-irradiated Titanium Dioxide at Room Temperature. *The Journal of Physical Chemistry A*, **83**, 2251-2255. https://doi.org/10.1021/j100480a014

[19] Ye, J., Liu, S.Q., Liu, W.X., Da Meng, Z., Luo, L., Chen, F. and Zhou, J. (2019) Photocatalytic Simultaneous Removal of Nitrite and Ammonia via a Zinc Ferrite/Activated Carbon Hybrid Catalyst under UV-Visible Irradiation. *ACS Omega*, **4**, 6411-6420. https://doi.org/10.1021/acsomega.8b00677

[20] Shibuya, S., Aoki, S., Sekine, Y. and Mikami, I. (2013) Influence of Oxygen Addition on Photocatalytic Oxidation of Aqueous Ammonia over Platinum-Loaded TiO_2. *Applied Catalysis B: Environmental*, **138-139**, 294-298. https://doi.org/10.1016/j.apcatb.2013.03.003

[21] Zhao, J., Li, N., Yu, R., Zhao, Z. and Nan, J. (2018) Magnetic Field Enhanced Denitrification in Nitrate and Ammonia Contaminated Water under 3D/2D Mn_2O_3/g-C_3N_4 Photocatalysis. *Chemical Engineering Journal*, **349**, 530-538. https://doi.org/10.1016/j.cej.2018.05.124

[22] Bahmani, M., Dashtian, K., Mowla, D., Esmaeilzadeh, F. and Ghaedi, M. (2020) UiO-66(Ti)-Fe_3O_4-WO_3 Photocatalyst for Efficient Ammonia Degradation from Wastewater into Continuous Flow-Loop Thin Film Slurry Flat-Plate Photoreactor. *Journal of Hazardous Materials*, **393**, Article ID: 122360. https://doi.org/10.1016/j.jhazmat.2020.122360

[23] Fujishima, A., Rao, T.N. and Tryk, D.A. (2000) Titanium Dioxide Photocatalysis. *Journal of Photochemistry and Photobiology C: Photochemistry Reviews*, **1**, 1-21. https://doi.org/10.1016/S1389-5567(00)00002-2

[24] Gaya, U.I. and Abdullah, A.H. (2008) Heterogeneous Photocatalytic Degradation of Organic Contaminants over Titanium Dioxide: A Review of Fundamentals, Progress and Problems. *Journal of Photochemistry and Photobiology C: Photochemistry Reviews*, **9**, 1-12. https://doi.org/10.1016/j.jphotochemrev.2007.12.003

[25] Banerjee, S., Pillai, S.C., Falaras, P., O'Shea, K.E., Byrne, J.A. and Dionysiou, D.D. (2014) New Insights into the Mechanism of Visible Light Photocatalysis. *The Journal of Physical Chemistry Letters*, **5**, 2543-2554. https://doi.org/10.1021/jz501030x

[26] Kosslick, H., Wang, Y., Ibad, M.F., Guo, X., Lütgens, M., Lochbrunner, S., Frank, M., Liem, N.Q. and Schulz, A. (2021) High-Performance Room-Light-Driven β-$AgVO_3$/mpg-C_3N_4 Core/Shell Photocatalyst Prepared by Mechanochemical Method. *Advances in Chemical Engineering and Science*, **11**, 290-315. https://doi.org/10.4236/aces.2021.114018

[27] Ortiz, N., Lima Azevedo, I.R.C., Vieira, M.G., Maichin, F. and Nascimento, L. (2020) Oxytetracycline Water Contamination Treated with Biocarbon TiO_2 and Solar Photodecomposition. *Journal of Agricultural Chemistry and Environment*, **9**, 299-313. https://doi.org/10.4236/jacen.2020.94022

[28] Hu, G., Cao, J., Wang, C., Lu, M. and Lin, Z. (2020) Study on the Characteristics of Naturally Formed TiO_2 Nanoparticles in Various Surficial Media from China. *Chemical Geology*, **550**, Article ID: 119703. https://doi.org/10.1016/j.chemgeo.2020.119703

[29] Mohammed Bukar, A., Mohammed El-Jummah, A. and Hammajam, A.A. (2022) Development and Evaluation of the Mechanical Properties of Coconut Fibre Reinforced Low Density Polyethylene Composite. *Open Journal of Composite Materials*, **12**, 83-97. https://doi.org/10.4236/ojcm.2022.123007

[30] Tao, Y., Han, Z., Cheng, Z., Liu, Q., Wei, F., Ting, K.E. and Yin, X.J. (2015) Synthesis of Nanostructured TiO_2 Photocatalyst with Ultrasonication at Low Temperature. *Journal of Materials Science and Chemical Engineering*, **3**, 29-36. https://doi.org/10.4236/msce.2015.31005

[31] Ndengue, M.J., Ayissi, M.Z., Noah, P.M.A., Ebanda, F.B. and Ateba, A. (2021) Implementation and Evaluation of Certain Properties of a Polymer Matrix Composite Material Reinforced by Fibrous Residues of *Saccharum officinarum* in View of an Applicability Orientation. *Journal of Minerals and Materials Characterization and Engineering*, **9**, 206-225. https://doi.org/10.4236/jmmce.2021.92015

[32] Ahuja, T., Brighu, U. and Saxena, K. (2023) Recent Advances in Photocatalytic Materials and Their Applications for Treatment of Wastewater: A Review. *Journal of Water Process Engineering*, **53**, Article ID: 103759. https://doi.org/10.1016/j.jwpe.2023.103759

[33] Mohammad, A.W., Teow, Y.H., Chong, W.C. and Ho, K.C. (2019) Chapter 13—Hybrid Processes: Membrane Bioreactor. In: Ismail, A.F., Rahman, M.A., Othman, M.H.D. and Matsuura, T., Eds., *Membrane Separation Principles and Applications*, Elsevier, Amsterdam, 401-470. https://doi.org/10.1016/B978-0-12-812815-2.00013-2

[34] Nakamoto, K., Ohshiro, M. and Kobayashi, T. (2017) Mordenite Zeolite—Polyethersulfone Composite Fibers Developed for Decontamination of Heavy Metal Ions. *Journal of Environmental Chemical Engineering*, **5**, 513-525. https://doi.org/10.1016/j.jece.2016.12.031

[35] Ooshiro, M., Kobayashi, T. and Uchida, S. (2017) Fibrous Zeolite-Polymer Composites for Decontamination of Radioactive Waste Water Extracted from Radio-Cs Fly Ash. *International Journal of Engineering and Technical Research*, **7**.

[36] Kobayashi, T., Ohshiro, M., Nakamoto, K. and Uchida, S. (2016) Decontamination of Extra-Diluted Radioactive Cesium in Fukushima Water Using Zeolite-Polymer Composite Fibers. *Industrial & Engineering Chemistry Research*, **55**, 6996-7002. https://doi.org/10.1021/acs.iecr.6b00903

[37] John, A.K., Palaty, S. and Sharma, S.S. (2020) Greener Approach towards the Synthesis of Titanium Dioxide Nanostructures with Exposed {001} Facets for Enhanced Visible Light Photodegradation of Organic Pollutants. *Journal of Materials Science: Materials in Electronics*, **31**, 20868-20882. https://doi.org/10.1007/s10854-020-04602-1